Carbohydrate Polymers 106 (2014) 34–41

Contents lists available at ScienceDirect

Carbohydrate Polymers

journal homepage: www.elsevier.com/locate/carbpol

Nanogel and superparamagnetic nanocomposite based on sodium alginate for sorption of heavy metal ions

Moslem Mansour Lakouraj*, Fatemeh Mojerlou, Ehsan Nazarzadeh Zare

Department of Organic-Polymer Chemistry, Faculty of Chemistry, University of Mazandaran, 47416 Babolsar, Iran

ARTICLE INFO

Article history:
Received 28 November 2013
Received in revised form 21 January 2014
Accepted 28 January 2014
Available online 5 February 2014

Keywords:
Nanogel
Superparamagnetic nanocomposite
Sodium alginate
Tetrasodium thiacalix[4]arene tetrasulfonate
Sorption
Heavy metal ions

ABSTRACT

Novel sodium alginate supported tetrasodium thiacalix[4]arene tetrasulfonate (TSTC[4]AS-s-SA) nanogel was prepared using sodium alginate nanoparticles. Then, superparamagnetic nanocomposite of sodium alginate (Fe_3O_4@TSTC[4]AS-s-SA) was fabricated from coprecipitation of sodium alginate supported tetrasodium thiacalix[4]arene tetrasulfonate and in situ generated Fe_3O_4 nanoparticles. Structural, morphological, surface, thermal and magnetic properties of the nanoadsorbents were studied by Fourier transform infrared (FT-IR), X-ray diffraction (XRD), scanning electron microscopy (SEM), transmission electron microscopy (TEM), atomic force microscopy (AFM), differential scanning calorimetry (DSC), thermal gravimetric analysis (TGA), and vibrating sample magnetometer (VSM), respectively. Adsorptions of Cu(II), Cd(II), Pb(II), Co(II), Ni(II) and Cr(III) ions onto nanoadsorbents were studied in aqueous condition at pH = 7. The results indicated that incorporation of thiacalix[4]arene tetrasulfonate and Fe_3O_4 into sodium alginate nanoparticles increased the adsorption capacity of sodium alginate bioadsorbents, and led to the magnetic property. The TSTC[4]AS-s-SA nanogels consist of rod-like structure with an average diameter of 50 nm.

1. Introduction

The pollution of water from toxic compounds, heavy metal ions and dyes imposes ecological and public problem due to hazardous and irrecoverable effects of such pollutants on human health and the environment (El-Sherbiny, Abdel-Hamid, Rashad, Ali, & Azab, 2013; Fu & Wang, 2011). Nowadays, a number of promising processes are used for elimination of heavy metal ions and dyes from wastewaters. Adsorption is a convenient separation process, in which the adsorbent may be of organic, mineral or natural source (Wan Ngah, Teong, & Hanafiah, 2011). Various materials such as zeolites, activated carbon, clays, agricultural wastes, biomass and synthetic polymers were used as an adsorbent (Karami, 2013; Tirtom, Dinçer, Becerik, Aydemir, & Çelik, 2012). However, these sorbents suffer from several problems such as low mechanical and thermal stability, high cost and poor sorption capacity. It is well known that biopolymers which are abundant, biodegradable and renewable resources have a high capacity to bind with a variety of waste molecules or ions through chemical and physical interactions. Among them, polysaccharide type biopolymers such as cellulose, chitosan, cyclodextrin, sodium alginate (SA) have received more attention (Honarkar & Barikani, 2009; Li et al., 2013; Trellenkamp & Ritter, 2010). SA, the salt of alginic acid composed of guluronic and mannuronic acid residues has been used as adsorbent for the removal of pollutants from wastewaters due to excellent hydrophilicity, binding ability, low cost, biocompatibility and renewability (Abdel-Halim & Al-Deyab, 2011; Li et al., 2013).

In the other hand, macrocyclic compounds were broadly used in host–guest chemistry for the manufacture of various receptors in charged or neutral molecules (Li, Zhan, Chen, Tian, & Zou, 2009). Thiacalix[4]arenes are macrocyclic oligomers that can exist in a relatively rigid and stable cone structure, consisting four phenol units linked by sulfur bridges (Garg, Bisht, & Chauhan, 2010). The cavity shape and self-assembling nature of these macromolecules have led to their wide application in the fields of molecular recognition and supramolecular chemistry. For instance, recently immobilized calixarenes on polymeric beds have been used as adsorbent for removal of toxic metal cations from water (Aksoy, Erdemir, Yildiz, & Yilmaz, 2012; Bozkurt, Kocabas, Durmaz, Yilmaz, & Sirit, 2009; Lakouraj & Tashakkorian, 2013; Li et al., 2009; Tabakci & Yilmaz, 2008).

Presently, magnetic nanoparticles (MNPs) have attracted the attention of scientists because of their unique application in biology, physics, materials science and especially in biomedical application including magnetic drug targeting, enzyme immobilization and magnetic resonance imaging contrasting agent (Bozkurt et al., 2009; Gupta & Gupta, 2005; Singh, Kalita, Singh, & Malhotra, 2011). In wastewater treatment, magnetic separation method has some advantages, such as high efficiency and cost-effectiveness (Unsoy, Yalcin, Khodadust, Gunduz, & Gunduz, 2012).

* Corresponding author. Tel.: +98 1125342350; fax: +98 1125342350.
E-mail address: lakouraj@umz.ac.ir (M.M. Lakouraj).

0144-8617/$ – see front matter © 2014 Elsevier Ltd. All rights reserved.
http://dx.doi.org/10.1016/j.carbpol.2014.01.092

Magnetic adsorbents are usually composed of the magnetic cores to ensure a strong magnetic response and a polymeric shell to supply favorable functional groups for various applications (Hua et al., 2012; Xu et al., 2012). More recently, polymeric-multifunctional nanocomposites with magnetic property have received great attention, and study on the composites has become one of the most attractive and promising research areas (Gong et al., 2012; Hua et al., 2012; Li et al., 2013; Yuwei & Jianlong, 2011; Zhang et al., 2010).

In order to make high performance multifunctional nanoadsorbent with controllable paramagnetic property and to elimination the heavy metal ions by simple filtration, we have introduced, novel, inexpensive, and eco-friendly nanobiosorbents to remove the ionic pollutants in wastewater using nanogel of tetrasodium thiacalix[4]arene tetrasolfonate supported sodium alginate (TSTC[4]AS-s-SA). Then, to enhance the adsorption capacity and ease of separation, the Fe_3O_4@TSTC[4]AS-s-SA magnetic nanocomposite was prepared via in situ coprecipitation technique using Fe(II) and Fe(III) salts in the presence of thiacalix[4]arene tetrasolfonate supported sodium alginate (TSTC[4]AS-s-SA). We have characterized the nanosorbents and investigated the materials properties, by Fourier transform infrared (FT-IR), X-ray diffraction (XRD), scanning electron microscopy (SEM), Transmission electron microscopy (TEM), atomic force microscopy (AFM), differential scanning calorimetry (DSC), thermal gravimetric analysis (TGA), and vibrating sample magnetometer (VSM). Furthermore, their application for sorption of some frequently encountered heavy metal cations such as Cu(II), Cd(II), Pb(II), Co(II), Ni(II) and Cr(II) were investigated.

2. Experimental

2.1. Materials

Sodium alginate (M_w = 60,000–80,000, and M/G = 32/68) and N,N′-diisopropylcarbodiimide (DIC, coupling reagent) were purchased from Aldrich. Analytical-reagent grade of $Co(NO_3)_2$, $Cd(NO_3)_2$, $Cu(NO_3)_2$, $Ni(NO_3)_2$, $Pb(NO_3)_2$, $Cr(NO_3)_3$ and other chemicals including HCl, NaOH, sulfur (S_8), $FeCl_3{\cdot}6H_2O$, $FeCl_2{\cdot}4H_2O$, triethylamine (TEA), adipoyl chloride (AC) and all solvents were purchased from Merck (Germany).

2.2. Preparation of sodium alginate (SA) nanoparticles

For preparation of SA nanoparticles, firstly 5 g of SA was pulverized by mortar to obtain a homogeneous free flowing powder. Then, the obtained SA powder was placed in a round-bottomed flask equipped with inlet and outlet of N_2 under sonication bath with agitation 53 KHz at room temperature for 2 h.

2.3. Synthesis of p-tert-butylthiacalix[4]arene (p-BTC[4]A)

p-BTC[4]A was prepared based on already reported method (Iki, Kabuto, Fukushima, Kumagai, & Takeya, 2000).

m.p: 320–322 °C (Lit. (Iki et al., 2000) 320–322 °C)
FT-IR (KBr, ν cm^{-1}): 3251(O—H), 2963 (C—H), 1638 (C=C), 1457 (C—H), 1130 (C—O), 680 cm^{-1}(C—S)
^{1}H NMR (400 MHz, $CDCl_3$): δ 9.52 (s, 4H, OH), δ 7.56 (s, 8H, ArH), δ 1.24 (s, 36H, *t*-Bu)
^{13}C NMR (400 MHz, $CDCl_3$): δ 155.6. 144.7, 136.4, 120.5 (C, Ar), δ 34.2 (C, *t*-Bu), δ 31.2 (C, *t*-Bu)

2.4. Synthesis of tetrasodium thiacalix[4]arene tetrasulfonate (TSTC[4]AS)

TSTC[4]AS was synthesized based on the literature method (Yuan, Zhu, Ma, & Yan, 2002). Firstly, 1.5 g of *p*-BTC[4]A was mixed with 80 mL of concentrated sulfuric acid, and the suspension was heated at 80 °C for 4 h under stirring. The solution was cooled and poured into 500 mL of ice-water (4:1) mixture, and the purple solid residue was filtered. Then, 100 g of sodium chloride was added to the filtrate to afford sodium salt. The salt was dried and dissolved in water, then ethanol was added to form a milky precipitate. The white precipitate was dried in vacuum oven at 60 °C for 24 h.

m.p: 300 °C (Lit (Yuan et al., 2002) 300 °C)
FT-IR (KBr, ν cm^{-1}): 3335 (OH), 1390 and 1139 (SO_3)
^{1}H NMR (400 MHz, DMSO): δ 10.64 (s, 4H, OH), δ 7.73 (s, 8H, ArH)
^{13}C NMR (400 MHz, $CDCl_3$): δ 138.68, 134.24, 128.64, 120.64, 56.41, 19.02

2.5. Synthesis of TSTC[4]AS-s-SA nanogel

In a round-bottomed flask, about 6.0 g of SA nanoparticles, 2.55 g TSTC[4]AS, and 0.37 mL DIC as a coupling reagent were mixed in 150 mL of dry DMSO. The flask was kept under continuous agitation using magnetic stirrer (at 1500 rpm) under N_2 atmosphere for three days. After that, 0.03 mL AC as a cross-linker and 0.06 mL TEA as a catalyst were added to the reaction mixture and stirred for three days more. Then, 100 mL of acetone was added to the obtained viscose solution. The resulting mixture was filtered and the filter cake was dried in vacuum oven for 3 h at 45 °C to give TSTC4AS-s-SA nanogel in 64.5% yield. The same procedure, without addition of cross-linker and TEA, was used to prepare the TSTC[4]AS supported SA (uncross-linked TSTC4AS-s-SA) as a soluble hydrogel.

2.6. Synthesis of superparamagnetic Fe_3O_4@TSTC[4]AS-s-SA nanocomposite

Superparamagnetic Fe_3O_4@TSTC[4]AS-s-SA nanocomposite was synthesized from a mixture solution of Fe(II) and Fe(III) salts and uncross-linked TSTC[4]AS-s-SA hydrogel via in situ co-precipitation method. Briefly, 0.994 g of $FeCl_2{\cdot}4H_2O$ and 2.73 g of $FeCl_3{\cdot}6H_2O$ were dissolved in 25 mL deionized water at room temperature. Then 1 g of uncross-linked TSTC[4]AS-s-SA was added to above solution and the mixture was stirred mechanically at 80 °C for 15 min. 10 mL NH_4OH (25%) was quickly added into the mixture until the pH reached to 10. After 30 min, the black precipitate was separated by magnetic decantation and washed several times with deionized water and twice with ethanol. Finally, Fe_3O_4@TSTC[4]AS-s-SA nanocomposite was dried at 80 °C under vacuum for 6 h.

2.7. Adsorption experiments

Adsorption experiments were performed for TSTC[4]AS-s-SA nanogel and superparamagnetic Fe_3O_4@TSTC[4]AS-s-SA nanocomposite by mixing 0.2 g of nanoabsorbent with 50 mL metal ions solution (50 ppm) in a flask. The pH of solutions was adjusted by adjustment with 1 M HCl or 1 M NaOH solution using a pH meter. The mixture was magnetically stirred at room temperature for 2 h. When the adsorption experiment was completed, the mixture was filtered, and the concentration of cations before and after adsorption was measured by AAS. The adsorption percentage of cations (*S*%) was calculated using following equation:

$$S\% = \left(\frac{C_i - C_e}{C_i}\right) \times 100$$

where C_i and C_e are the initial and final concentration of cation in the solution (mg/L) before and after sorption, respectively.

The adsorption capacity, q_t (mg/g), was calculated using the following equation:

$$q_t = \left(\frac{C_i - C_e}{m}\right) V$$

where, m (g) is the mass of nanoadsorbent and V (L) is volume of the cation solution.

2.8. Desorption experiment

For desorption experiment, aqueous solution of HCl (0.2 M) was used. The nanoadsorbents–ion complexes in which adsorption was carried out in pH = 7 were immersed in HCl solution (0.2 M) while being stirred at room temperature for 1 h. After filtration, the residual metal ion concentrations in the solution were determined by AAS. The desorption percentage ($D\%$) was calculated as follows formula:

$$\%D = \frac{\text{mmoles of metal ions desorbed to the HCl solution}}{\text{mmoles of metal ions adsorbed on to resin}} \times 100$$

2.9. Characterizations

FT-IR analysis was carried out on a Bruker Tensor 27 spectrometer (Bruker, Karlsrohe, Germany). ^{1}H and ^{13}C NMR spectra were recorded on a 400 MHz Bruker Avance DRX Spectrometer in DMSO-d_6 and $CDCl_3$ using tetramethyl silane as an internal reference. The X-ray diffraction (XRD, Shibuya-ku, Japan) patterns were recorded at room temperature on a Riga kuD/Max-2550 powder diffractometer with a scanning rate of 5° min^{-1}, and recorded in the 2θ range of 10–70 °C. Thermo-gravimetric analysis of prepared nanoadsorbents was investigated using the LENSES STAPT-1000 calorimeter (Germany) by scanning up to 700 °C with the heating rate of 10 °C/min. Differential Scanning Calorimetry (DSC) analysis of the prepared nanoadsorbents was performed with Elmerpyris Diamond Perkin Calorimeter (Germany) with scanning up to 700 °C at a heating rate of 10 °C/min. VSM measurement was performed by using a Vibrating sample magnetometer Daghigh Kavir Corporation. The magnetization measurements were carried out in an external field up to 15 kOe at room temperature. Sonication agitation was carried out on a Soner 220H Ultrasonic Cleaner, AC110V, 60 Hz (Taiwan). Scanning electron microscopy (SEM) was recorded on a Hitachi S4160 instrument. Transmission electron microscopy (TEM) observations were performed on a CM1 electron microscope at an accelerating voltage of 120 kV (Philips, The Netherlands). Atomic force microscopy (AFM) measurements were performed on a Nanosurf easy Scan2 Flex AFM (made of Switzerds).

3. Results and discussion

Schematic illustration of the synthetic procedure and the overall structure of TSTC[4]AS-s-SA nanogel (A) and Fe_3O_4@TSTC[4]AS-s-SA superparamagnetic nanocomposite (B) are represented in Scheme 1.

3.1. FT-IR

The FT-IR spectra of, SA, TSTC[4]AS, bare Fe_3O_4 nanoparticles, TSTC[4]AS-s-SA nanogel and Fe_3O_4@TSTC[4]AS-s-SA nanocomposite are presented in Fig. 1. The FT-IR spectra of SA displays absorption band at 1106 cm^{-1} corresponding to stretching vibration of its C—OH groups (Mandal & Ray, 2013). The band around 1025 cm^{-1} (C—O—C stretching) presenting in the IR

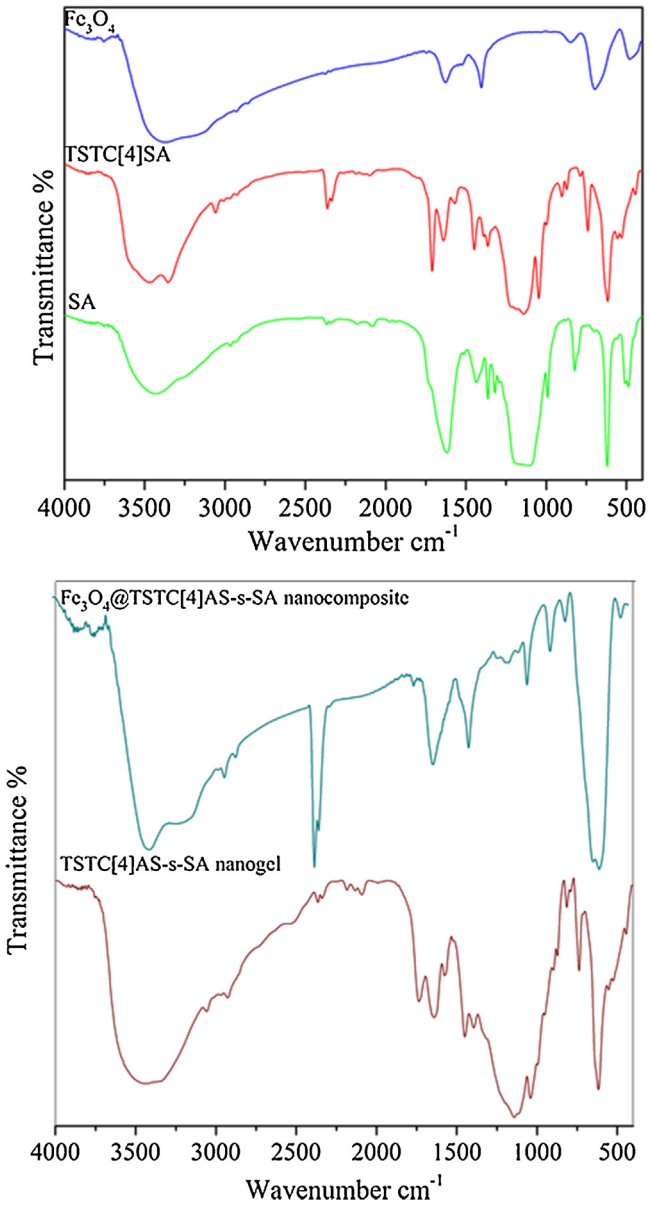

Fig. 1. FT-IR spectra of SA, TSTC[4]AS, Fe_3O_4 nanoparticles, TSTC[4]AS-s-SA nanogel and Fe_3O_4@TSTC[4]AS-s-SA nanocomposite.

spectrum of sodium alginate is attributed to its glucosidal linkages. Two absorption bands around 1600 and 1400 cm^{-1} can be attributed to asymmetric and symmetric stretching vibrations of carboxylate group, respectively (Srivastava et al., 2012). The strong peak at 3350 cm^{-1} is due to OH stretching vibrations.

The TSTC[4]AS exhibits four main stretching vibration bands at 3335, 3100, 1390 and 1139 cm^{-1} corresponding to stretching vibration of hydroxyl, aromatic C—H and sulfonates groups, respectively (Yuan et al., 2002). The characteristic absorption band of Fe_3O_4 nanoparticles at 667 cm^{-1} is assigned to Fe—O—Fe bonds (Lakouraj, Zare, & Moghadam, 2014; Srivastava et al., 2012). The peak at 3383 cm^{-1} confirms existence of hydroxyl groups on the surface of the Fe_3O_4. In FT-IR spectra of TSTC[4]AS-s-SA, peak at 3447 cm^{-1} assigned to hydroxyl groups. The peaks at 1040 and 1735 cm^{-1} approved the etheric and esteric bond formation. Also the peaks at 2800 and 3080 cm^{-1} are related to aliphatic and aromatic C—H in nanogel. In addition, the peak of stretching vibration of the sulfonate (expected at around 1180 cm^{-1}) was also submerged by SA

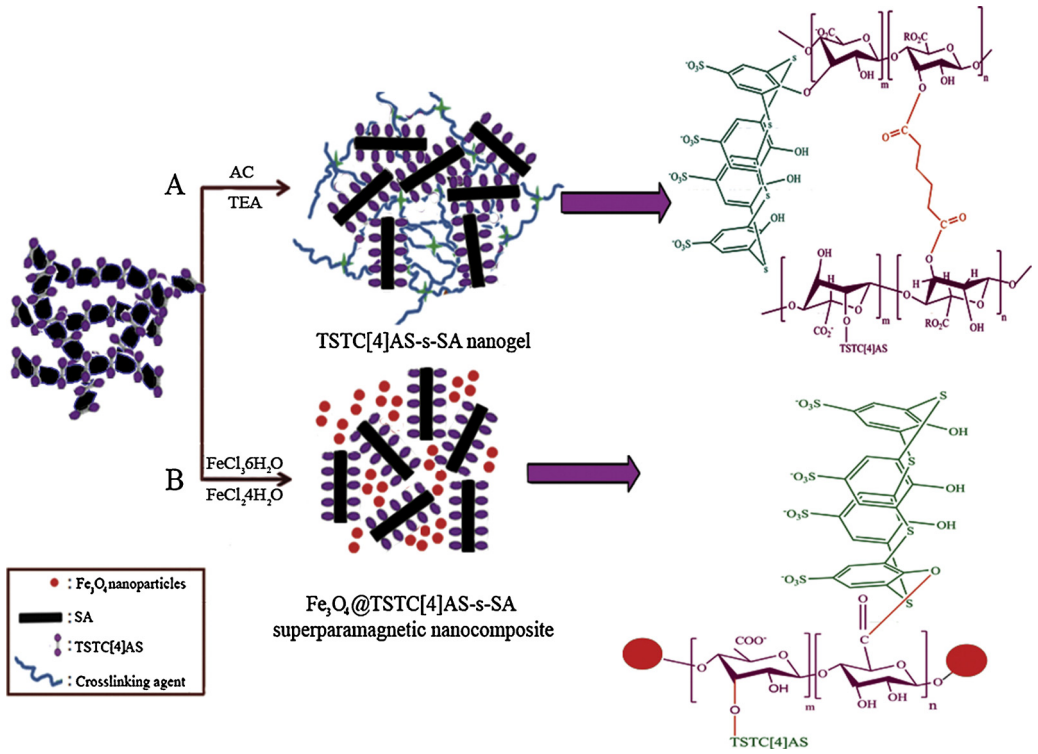

Scheme 1. Schematic illustration of the synthetic procedure and the overall structure of TSTC[4]AS-s-SA nanogel (A) and Fe_3O_4@TSTC[4]AS-s-SA superparamagnetic nanocomposite (B).

ring absorptions. These absorption bands confirm that TSTC[4]AS was firmly linked on SA. The FT-IR spectra of the Fe_3O_4@TSTC[4]AS-s-SA nanocomposite almost contain characteristic peaks of the components, of which a broad and strong vibration bond at about 3421–3120 cm^{-1} represents the overlapping of stretching vibrational bands of phenolic OH and hydroxyl groups on alginate (of pyranose rings) and those of magnetite surface. Other characteristic absorption bands of SA (2924, 1619 and 618 cm^{-1}), Fe_3O_4 (585 cm^{-1}) and TSTC[4]AS (3050, 1730, 1400, and 1035 cm^{-1}) are evident in the spectrum of Fe_3O_4@TSTC[4]AS-s-SA nanocomposite.

3.2. XRD

Fig. 2 shows the XRD patterns of SA, Fe_3O_4 nanoparticles, TSTC[4]AS-s-SA and superparamagnetic Fe_3O_4@TSTC[4]AS-s-SA nanoadsorbents. As seen in Fig. 2, the diffraction peaks at $2\theta = 12.02°, 13.13°, 18.30°, 20.28°, 21.35°, 24.18°, 28.11°$ and $38.19°$ correspond to semi-crystalline nature of SA. In XRD pattern of Fe_3O_4 nanoparticles, the characteristic peaks were observed at $2\theta = 13.12°, 19.60°, 20.25°, 27.20°, 29.35°, 30.05°, 38.39°$ and $40.15°$ which imply the crystalline nature of Fe_3O_4 nanoparticles. There are a lot of peaks at $2\theta = 15.10°, 17.08°, 19.21°, 21.14°, 23.81°$ and 25.66 for TSTC[4]AS-s-SA nanogel which revealed semi-crystalline nature for TSTC[4]AS-s-SA nanogel. The XRD pattern of superparamagnetic Fe_3O_4@TSTC[4]AS-s-SA nanocomposite depicts sharp peaks at $2\theta = 19.16°, 22.01°, 24.11°, 26.84°, 29.48°, 31.72°, 34.60°, 35.64°, 38.56°, 40.16°, 46.26°$ and $48.76°$ as shown in Fig. 2. The crystalline nature of nanocomposite seems to be improved probably due to the regular interaction of the TSTC[4]AS-s-SA with Fe_3O_4 nanoparticles and ordered alignment of the nanorods. The average crystal size of the nanocomposite can be calculated according to Scherrer's equation (Osuna et al., 2012). Our results demonstrated that according to Scherer equation, the mean diameter of nanoparticles in the nanocomposite approximately was 22.36 nm.

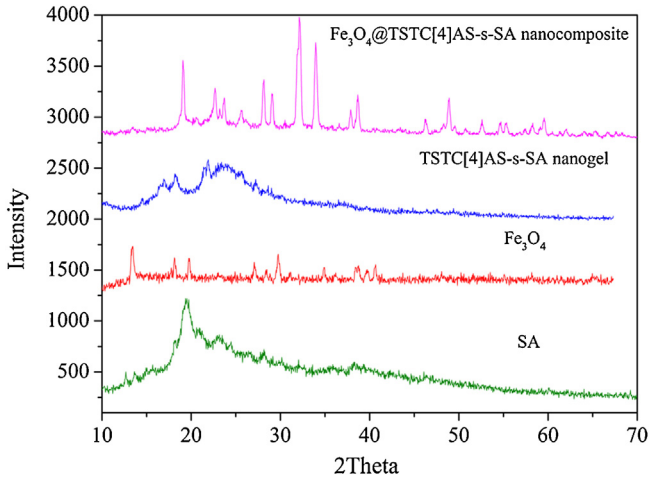

Fig. 2. XRD patterns of SA, Fe_3O_4 nanoparticles, TSTC[4]AS-s-SA nanogel and Fe_3O_4@TSTC[4]AS-s-SA nanocomposite.

3.3. SEM and TEM analysis

Morphology and particle size of the SA nanoparticles, TSTC[4]AS-s-SA nanogel and Fe_3O_4@TSTC[4]AS-s-SA magnetic nanocomposite adsorbents were investigated by SEM (a, b, c, e) and TEM (d and f), and the images are shown in Fig. 3. As seen in Fig. 3a and b, they reveal that the SA particles have irregular surfaces of densely polyhedral granules with a fairly different size distribution around 100–200 nm in average diameter. It is evident from Fig. 3c and d that TSTC[4]AS-s-SA nanoparticles consist exclusively of rod-like structure with an average diameter of 50 nm. It seem that linked TSTC[4]AS to SA nanoparticles caused formation of rod-like structures of nanogel. Fig. 3e and f represents a rod-like Fe_3O_4@TSTC[4]AS-s-SA nanocomposite in which

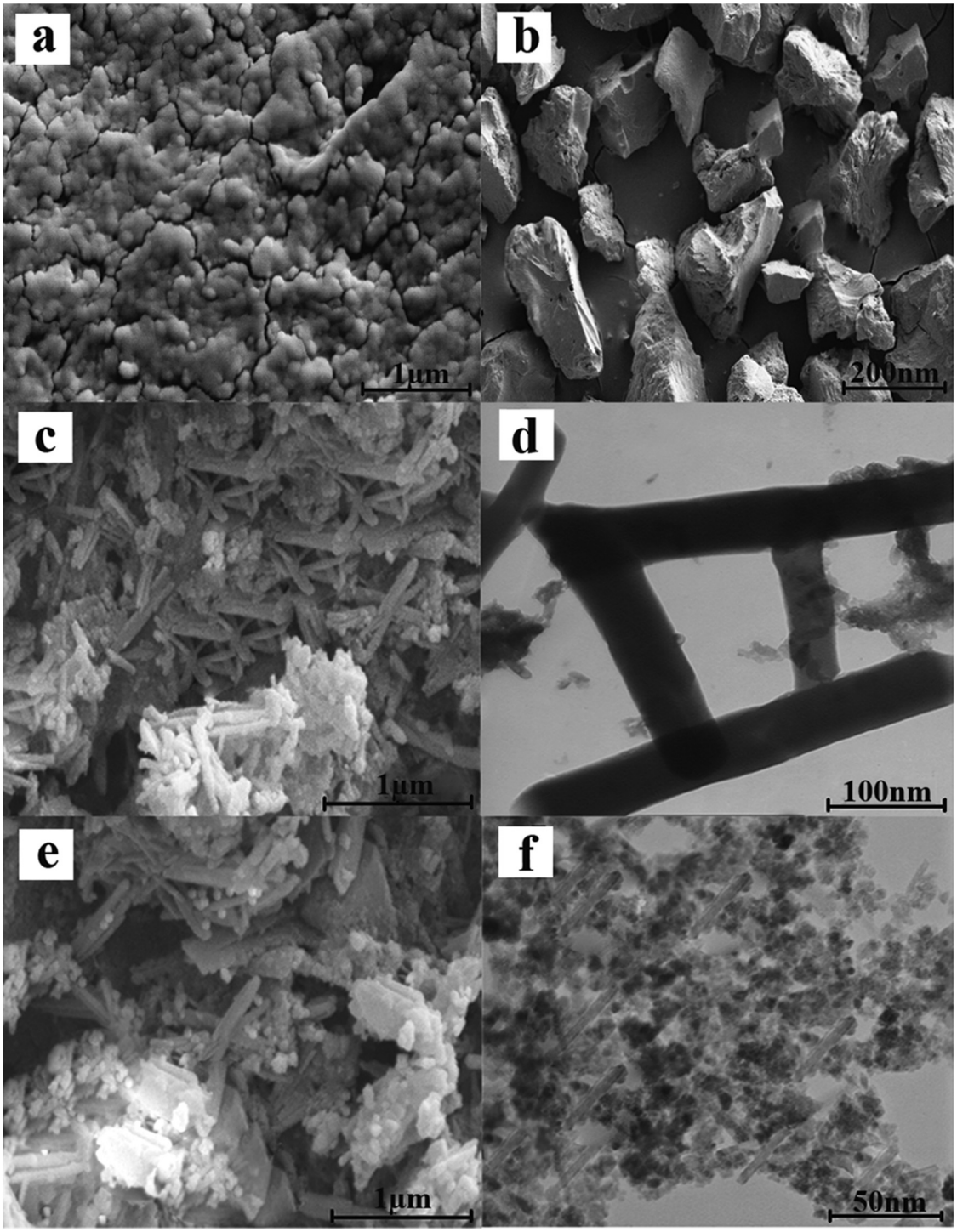

Fig. 3. SEM images (a and b) of SA nanoparticles, SEM and TEM images (c and d) of TSTC[4]AS-s-SA nanogel, and (e and f) for Fe_3O_4@TSTC[4]AS-s-SA nanocomposite.

the Fe_3O_4 nanoparticles are randomly dispersed in TSTC[4]AS-s-SA matrix. Apparently, the particle size of TSTC[4]AS-s-SA nano-rod and Fe_3O_4 nanoparticles is 25 nm and 10 nm, respectively.

3.4. AFM analysis

To observe morphological properties such as surface porosity, roughness and texture, micrographs of the surface and cross-section of the pure TSTC[4]AS-s-SA nanogel and Fe_3O_4@TSTC[4]AS-s-SA nanocomposite adsorbents were taken by using AFM. Fig. 4a and b shows TSTC[4]AS-s-SA and Fe_3O_4@TSTC[4]AS-s-SA images in 2-dimensional (2-D) and 3-dimensional (3-D). These images amazingly show surface homogeneity of the TSTC[4]AS-s-SA and Fe_3O_4@TSTC[4]AS-s-SA nanoadsorbents.

3.5. Magnetic properties

VSM is used to evaluate the magnetic properties of materials as a function of magnetic field, temperature, and time. Typical magnetization curves of the Fe_3O_4 nanoparticles and

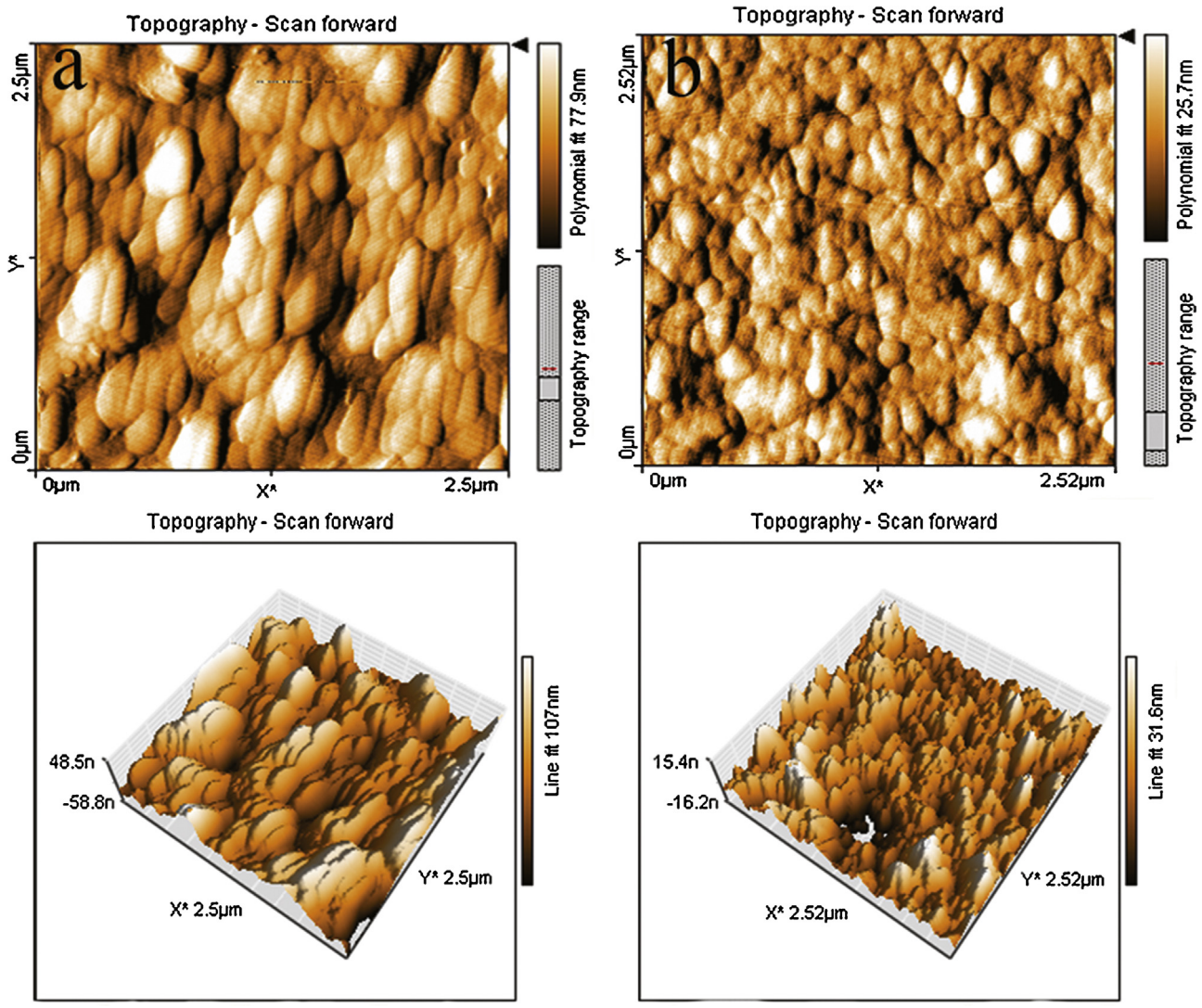

Fig. 4. AFM images of the (a) Fe_3O_4@TSTC[4]AS-s-SA nanocomposite (b) TSTC[4]AS-s-SA nanogel at 2-D and 3-D images.

Fe_3O_4@TSTC[4]AS-s-SA nanocomposite with the applied magnetic field are displayed in Fig. 5.

The result shows that Fe_3O_4 nanoparticles and Fe_3O_4@TSTC[4]AS-s-SA nanocomposite have superparamagnetic properties because of the both remanence (Mr) and coercivity (Hc) are near zero (Unsoy et al., 2012). Fe_3O_4@TSTC[4]AS-s-SA nanocomposite showed a smaller Hc and Mr compared to bare Fe_3O_4 nanoparticles. However, it can be concluded that the presence of TSTC[4]AS-s-SA on surface of Fe_3O_4 can reduce agglomeration of magnetic nanoparticles. The saturation magnetization (Ms) of pure Fe_3O_4 and Fe_3O_4@TSTC[4]AS-s-SA was 54 and 45.6 emu/g, respectively. It is well known that the energy of a magnetic particle in an external field is proportional to its size via the number of magnetic molecules in a single magnetic domain (Mohammadi, Barikani, & Barmar, 2013). When this energy becomes comparable to the thermal energy, thermal fluctuations near the surface of Fe_3O_4 nanoparticles cause magnetically disordered surface that will significantly reduce the total magnetic moments at a given field (Mohammadi et al., 2013). This phenomenon is more significant for the nanoparticles due to their large surface to volume ratio. Therefore, the smaller saturation magnetization value for the nanoparticles compared to the bulk materials is reasonable. Also surface modification of magnetic nanoparticles can also cause a slight decrease in saturation magnetization value for Fe_3O_4@TSTC[4]SA-s-SA nanocomposite compared to pure Fe_3O_4 nanoparticles.

3.6. Thermal properties of nanoadsorbents

Fig. 6a shows DSC curves of TSTC[4]AS-s-SA nanogel and Fe_3O_4@TSTC[4]AS-s-SA nanocomposite under N_2 atmosphere at the heating rate of 10 °C/min. In DSC curve of TSTC[4]AS-s-SA nanogel, the endothermic peak at 73 °C indicates the loss of entrapped water molecules in the networks which were not been removed during initial drying in the oven. The endothermic peak at 225 °C and exothermic peak at 390 °C can be related to melting temperature (T_m) and thermal decomposition. The DSC curve of Fe_3O_4@TSTC[4]AS-s-SA nanocomposite shows two endothermic peaks at 73 °C and 250 °C which correspond to dehydration and melting temperature, respectively. Comparison of DSC curve of TSTC[4]AS-s-SA nanogel and Fe_3O_4@TSTC[4]AS-s-SA nanocomposite shows that T_m and decomposition temperature in Fe_3O_4@TSTC[4]AS-s-SA nanoadsorbent were improved. To confirm this claim, thermo-gravimetric analysis was taken of TSTC[4]AS-s-SA nanogel and Fe_3O_4@TSTC4AS-s-SA nanocomposite. Fig. 6b demonstrates TGA curves of TSTC[4]AS-s-SA nanogel and Fe_3O_4@TSTC[4]AS-s-SA nanocomposite under N_2 atmosphere at the heating rate of 10 °C/min. As can be seen in Fig. 6b,

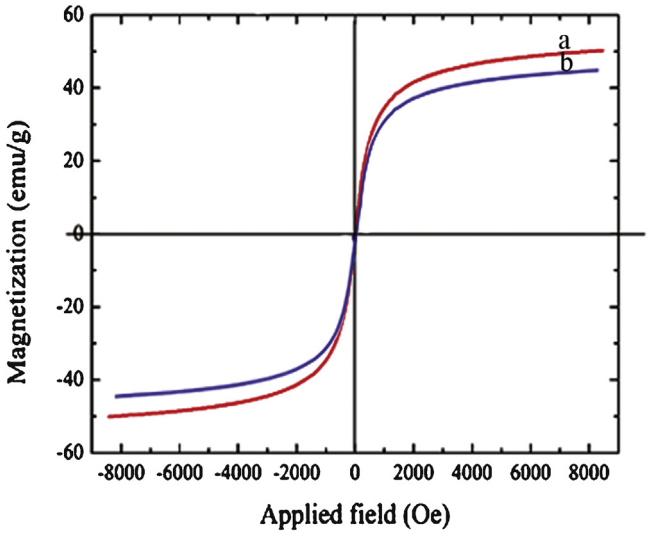

Fig. 5. VSM magnetization curves of pure Fe_3O_4 and Fe_3O_4@TSTC[4]AS-s-SA nanocomposite.

each TGA curves consist of three parts; the first part, the 2 wt% loss up to 100 °C for TSTC[4]AS-s-SA and 4 wt% loss at 102 °C for Fe_3O_4@TSTC[4]AS-s-SA sample are related to dehydration. The second part is a thermal degradation stage resulting from pyrolysis which started from about 300 °C and ended at 700 °C with loss of 55 wt% and 65 wt% for TSTC[4]AS-s-SA nanogel and Fe_3O_4@TSTC[4]AS-s-SA nanocomposite, respectively. The third part represents the conversion of the remaining materials to carbon residues. The residual weights are 50 wt% and 60 wt% at 800 °C for TSTC[4]AS-s-SA nanogel and Fe_3O_4@TSTC[4]AS-s-SA nanocomposite, respectively. These results showed that Fe_3O_4@TSTC[4]AS-s-SA nanocomposite have higher thermal stability than TSTC[4]AS-s-SA nanogel.

3.7. Determination of percent and capacity of sorption for metal ions

Owing to the thiacalix[4]arene cavity and functional groups of alginate, the nanogel of thiacalix[4]arenes/alginate and its magnetic nanocomposite have great potential for complex formation with a broad range of cations. That is to say, the carboxylate and sulfonate groups on the alginate and thiacalix[4]arene can enhance the ability of nanoadsorbents to coordinate tightly with metal cations. Thus, it is likely to be used for removal of ionic waste from water as a membrane or solid phase of fixed separating column.

Herein, we investigated the removal of some metal cations from aqueous media with the synthesized nanoadsorbents. It is well known that the sorption of metal ions depends on pH which extremely affects the chelation as well as physisorption processes (Molinari, Argurio, & Poerio, 2006). The sorption of all metal ions onto the nanoadsorbents was more favorable at pH of 7 since at low pH value, the carboxylate (COO^-) and sulfonate (SO_3^-) groups are in their protonated form. In addition, H^+ can compete with metal ions for sorption sites and reduces sorption capacity. At higher pH values, the OH^- competes with chelating groups in coordination to metal ions. Therefore, in this study we carried out the sorption experiments in neutral condition.

The sorption percentage and capacity of the synthetic TSTC[4]AS-s-SA nanogel and Fe_3O_4@TSTC[4]AS-s-SA nanocomposite for Pb(II), Cd(II), Co(II), Cu(II), Cr(II) and Ni(II) were evaluated in aqueous media at pH = 7 for 50 ppm concentration of ions. The results are summarized in Table 1.

It can be seen that the Fe_3O_4@TSTC[4]AS-s-SA nanocomposite, display high affinity for selected metal ions relative to TSTC[4]AS-s-SA nanogel. The effect of Fe_3O_4 on the sorption revealed that the sorption capacity increased significantly by Fe_3O_4 nanoparticles, in comparison with TSTC[4]AS-s-SA nanogel. It seems that incorporation of magnetic nanoparticles into TSTC[4]AS-s-SA caused increasing surface to volume ratio which increased the sorption capacity for Fe_3O_4@TSTC[4]AS-s-SA nanocomposite relative to TSTC[4]AS-s-SA. The order of sorption percentage changes as follows: Pb(II) > Cd(II) > Cu(II) > Cr(III) > Co(II) > Ni(II).

The results demonstrated that Fe_3O_4@TSTC[4]AS-s-SA nanocomposite and TSTC[4]AS-s-SA are effective candidates for sorption of such risky heavy metals especially for removing Pb^{2+} from wastewater which is one of the hazardous cations that cause some environmental concerns.

3.8. Desorption of metal ions from nanoadsorbents

Desorption value of the adsorbed metal cations from the nanoadsorbents was also investigated in a group experimental system. The nanoadsorbent beads loading to maximum amounts of the relevant metal ions in pH = 7 were placed within the

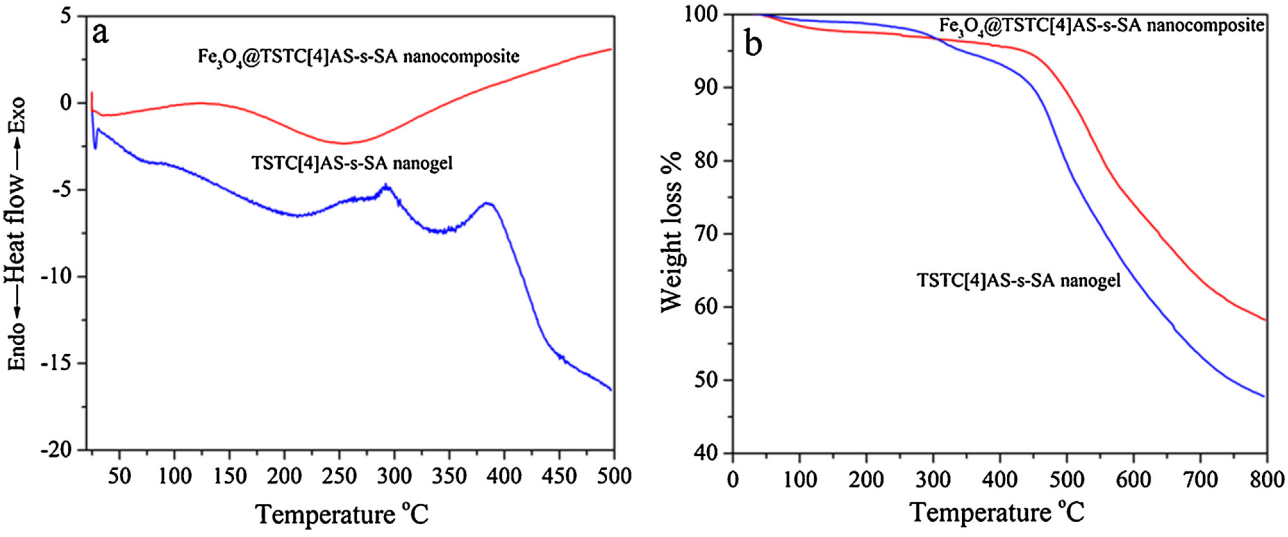

Fig. 6. (a) DSC and (b) TGA thermograms of TSTC[4]AS-s-SA nanogel and Fe_3O_4@TSTC[4]AS-s-SA nanocomposite.

Table 1
Adsorption percentage and capacity of the nanoadsorbents in 50 ppm test solution.

Nanoadsorbents	Co^{2+}	Cd^{2+}	Pb^{2+}	Cu^{2+}	Ni^{2+}	Cr^{3+}
Adsorption percentage (adsorption capacity)						
TSTC[4]AS-s-SA	64.5 (12.9)	89.14 (17.82)	84.5 (16.9)	87.82 (17.56)	62.9 (12.58)	77.3 (15.46)
Fe_3O_4@TSTC[4]AS-s-SA	74.9 (14.98)	94.5 (18.9)	99.8 (19.96)	90.56 (18.11)	67.4 (13.48)	79.2 (15.48)

desorption medium containing solution of HCl (0.2 M), and the amount of metal cations desorbed in 1 h was calculated. The results shows that all recorded desorption percentages for the cations were in range of 87–96.5%.

4. Conclusion

Superparamagnetic nanocomposite and nanogel as effective nanosorbents based on SA were synthesized. The chemical structures of nanoadsorbents were characterized by FT-IR spectroscopy. It is evident that a rod-like morphology is imaged with SEM and TEM for nanoadsorbents. Surprisingly, the nanoadsorbents showed high thermal stability and crystalline nature. VSM analysis exhibited that Fe_3O_4@TSTC[4]AS-s-SA nanocomposite has superparamagnetism property. Among the synthesized nanoadsorbents, Fe_3O_4@TSTC[4]AS-s-SA nanocomposite demonstrated higher affinity for the selected metal ions compared to TSTC[4]AS-s-SA nanogel, and the order of adsorption percentage changed as follows: Pb(II) > Cd(II) > Cu(II) > Cr(III) > Co(II) > Ni(II) at pH = 7. Based on efficient coordination ability of TSTC[4]AS with ions, we believe that present studies can be further extended to more complicated systems for encapsulation of different pollutant molecules such as ionic pigments, herbicides and fungicides.

References

Abdel-Halim, E. S., & Al-Deyab, S. S. (2011). Removal of heavy metals from their aqueous solutions through adsorption onto natural polymers. *Carbohydrate Polymers*, *84*(1), 454–458.

Aksoy, T., Erdemir, S., Yildiz, H. B., & Yilmaz, M. (2012). Novel water-soluble calix[4,6]arene appended magnetic nanoparticles for the removal of the carcinogenic aromatic amines. *Water Air, and Soil Pollution*, *223*(7), 4129–4139.

Bozkurt, S., Kocabas, E., Durmaz, M., Yilmaz, M., & Sirit, A. (2009). Synthesis and dichromate anion sorption of silica gel-immobilized calix[4]arenes. *Journal of Hazardous Materials*, *165*(1–3), 974–979.

El-Sherbiny, I. M., Abdel-Hamid, M. I., Rashad, M., Ali, A. S. M., & Azab, Y. a. (2013). New calcareous soil–alginate composites for efficient uptake of Fe(III), Mn(II) and As(V) from water. *Carbohydrate Polymers*, *96*(2), 450–459.

Fu, F., & Wang, Q. (2011). Removal of heavy metal ions from wastewaters: A review. *Journal of Environmental Management*, *92*(3), 407–418.

Garg, B., Bisht, T., & Chauhan, S. (2010). Ionic interactions of anionic thiacalix arene with cationic porphyrins. *Arkivoc*, 161–178.

Gong, J.-L., Wang, X.-Y., Zeng, G.-M., Chen, L., Deng, J.-H., Zhang, X.-R., & Niu, Q.-Y. (2012). Copper (II) removal by pectin–iron oxide magnetic nanocomposite adsorbent. *Chemical Engineering Journal*, *185/186*, 100–107.

Gupta, A. K., & Gupta, M. (2005). Synthesis and surface engineering of iron oxide nanoparticles for biomedical applications. *Biomaterials*, *26*(18), 3995–4021.

Honarkar, H., & Barikani, M. (2009). Applications of biopolymers I: Chitosan. *Monatshefte für Chemie – Chemical Monthly*, *140*(12), 1403–1420.

Hua, M., Zhang, S., Pan, B., Zhang, W., Lv, L., & Zhang, Q. (2012). Heavy metal removal from water/wastewater by nanosized metal oxides: A review. *Journal of Hazardous Materials*, *211/212*, 317–331.

Iki, N., Kabuto, C., Fukushima, T., Kumagai, H., & Takeya, H. (2000). Synthesis of p-tert-butylthiacalix[4]arene and its inclusion property. *Tetrahedron*, *56*, 1437–1443.

Karami, H. (2013). Heavy metal removal from water by magnetite nanorods. *Chemical Engineering Journal*, *219*, 209–216.

Lakouraj, M. M., & Tashakkorian, H. (2013). Synthesis of nanocrystalline polycalix[4]amides containing mesogenic triazole units and investigations of their thermo physical properties and heavy metal sorption behavior. *Journal of Macromolecular Science: Part A*, *50*(3), 310–320.

Lakouraj, M. M., Zare, E. N., & Moghadam, P. N. (2014). Synthesis of novel conductive poly(p-phenylenediamine)/Fe_3O_4 nanocomposite via emulsion polymerization and investigation of antioxidant activity. *Advances in Polymer Technology*, *33*(1), 21385.

Li, H., Zhan, J., Chen, M., Tian, D., & Zou, Z. (2009). Metal ions recognition by 1,2,3-triazolium calix[4]arene esters synthesized via click chemistry. *Journal of Inclusion Phenomena and Macrocyclic Chemistry*, *66*(1/2), 43–47.

Li, X., Qi, Y., Li, Y., Zhang, Y., He, X., & Wang, Y. (2013). Novel magnetic beads based on sodium alginate gel crosslinked by zirconium(IV) and their effective removal for Pb^{2+} in aqueous solutions by using a batch and continuous systems. *Bioresource Technology*, *142*, 611–619.

Mandal, B., & Ray, S. K. (2013). Synthesis of interpenetrating network hydrogel from poly(acrylic acid-co-hydroxyethyl methacrylate) and sodium alginate: Modeling and kinetics study for removal of synthetic dyes from water. *Carbohydrate Polymers*, *98*(1), 257–269.

Mohammadi, A., Barikani, M., & Barmar, M. (2013). Effect of surface modification of Fe_3O_4 nanoparticles on thermal and mechanical properties of magnetic polyurethane elastomer nanocomposites. *Journal of Materials Science*, *48*(21), 7493–7502.

Molinari, R., Argurio, P., & Poerio, T. (2006). Ultrafiltration of polymer–metal complexes for metal ion removal from wastewaters. *Macromolecular Symposia*, *235*(1), 206–214.

Osuna, Y., Gregorio-Jauregui, K. M., Gaona-Lozano, J. G., de la Garza-Rodríguez, I. M., Ilyna, A., Barriga-Castro, E. D., & López, R. G. (2012). Chitosan-coated magnetic nanoparticles with low chitosan content prepared in one-step. *Journal of Nanomaterials*, *2012*, 1–7.

Singh, J., Kalita, P., Singh, M. K., & Malhotra, B. D. (2011). Nanostructured nickel oxide–chitosan film for application to cholesterol sensor. *Applied Physics Letters*, *98*(12), 123702.

Srivastava, M., Singh, J., Yashpal, M., Gupta, D. K., Mishra, R. K., Tripathi, S., & Ojha, A. K. (2012). Synthesis of superparamagnetic bare Fe_3O_4 nanostructures and core/shell (Fe_3O_4/alginate) nanocomposites. *Carbohydrate Polymers*, *89*(3), 821–829.

Tabakci, M., & Yilmaz, M. (2008). Synthesis of a chitosan-linked calix[4]arene chelating polymer and its sorption ability toward heavy metals and dichromate anions. *Bioresource Technology*, *99*(14), 6642–6645.

Tirtom, V. N., Dinçer, A., Becerik, S., Aydemir, T., & Çelik, A. (2012). Comparative adsorption of Ni(II) and Cd(II) ions on epichlorohydrin crosslinked chitosan–clay composite beads in aqueous solution. *Chemical Engineering Journal*, *197*, 379–386.

Trellenkamp, T., & Ritter, H. (2010). Poly(N-vinylpyrrolidone) bearing covalently attached cyclodextrin via click-chemistry: Synthesis, characterization, and complexation behavior with phenolphthalein. *Macromolecules*, *43*(13), 5538–5543.

Unsoy, G., Yalcin, S., Khodadust, R., Gunduz, G., & Gunduz, U. (2012). Synthesis optimization and characterization of chitosan-coated iron oxide nanoparticles produced for biomedical applications. *Journal of Nanoparticle Research*, *14*(11), 964–977.

Wan Ngah, W. S., Teong, L. C., & Hanafiah, M. A. K. M. (2011). Adsorption of dyes and heavy metal ions by chitosan composites: A review. *Carbohydrate Polymers*, *83*(4), 1446–1456.

Xu, P., Zeng, G. M., Huang, D. L., Feng, C. L., Hu, S., Zhao, M. H., & Liu, Z. F. (2012). Use of iron oxide nanomaterials in wastewater treatment: A review. *Science of the Total Environment*, *424*, 1–10.

Yuan, D., Zhu, W.-X., Ma, S., & Yan, X. (2002). Bilayer structure of tetrasodium thiacalix[4]arene tetrasulfonate. *Journal of Molecular Structure*, *616*(1–3), 241–246.

Yuwei, C., & Jianlong, W. (2011). Preparation and characterization of magnetic chitosan nanoparticles and its application for Cu(II) removal. *Chemical Engineering Journal*, *168*(1), 286–292.

Zhang, L., Zhu, X., Sun, H., Chi, G., Xu, J., & Sun, Y. (2010). Control synthesis of magnetic Fe_3O_4–chitosan nanoparticles under UV irradiation in aqueous system. *Current Applied Physics*, *10*(3), 828–833.